Computational Correction for Imaging through Single Fresnel Lenses

Artem Nikonorov[1,2], Sergey Bibikov[1,2], Maksim Petrov[1], Yuriy Yuzifovich[1] and Vladimir Fursov[1,2]
[1]*Samara State Aerospace University, 34 Moskovskoe shosse, Samara, Russian Federation*
[2]*Image Processing Systems Institute of the RAS, 151 Molodogvardeyskaya str., Samara, Russian Federation*

Keywords: Fresnel Lens Imaging, Chromatic Aberration, Deconvolution, Deblur, Sharping, Color Correction, Total Variance Deblur.

Abstract: The lenses of modern single lens reflex (SLR) cameras may contain a dozen or more individual lens elements to correct aberrations. With processing power more readily available, the modern trend in computational photography is to develop techniques for simple lens aberration correction in post-processing. We propose a similar approach to remove aberrations from images captured by a single imaging Fresnel lens. The image is restored using three-stage deblurring of the base color channel, sharpening other and then applying color correction. The first two steps are based on the combination of restoration techniques used for restoring images obtained from simple refraction lenses. Color correction stage is necessary to remove strong color shift caused by chromatic aberrations of simple Fresnel lens. This technique was tested on real images captured by a simple lens, which was made as a three-step approximation of the Fresnel lens. Promising results open up new opportunities in using lightweight Fresnel lenses in miniature computer vision devices.

1 INTRODUCTION

Modern camera lenses have become very complex. They typically consist of a dozen elements or more necessary to remove optical aberrations (Meyer-Arendt, 1995). Recently, simple lenses with one or two optical elements were proposed (Heide et al., 2013). These lenses are similar to lenses used hundreds years ago, and chromatic aberration is still an issue for images captured using simple lenses (Heide et al., 2013). This aberration can now be corrected with digital processing.

A chromatic aberration is a correlation between optical system characteristics and a wavelength of the registered light. Chromatic aberrations result in a chroma in achromatic objects and/or in coloring the contours.

Lens producers use special arrays of low-dispersing elements to negate aberrations in imaging elements. The weight of these complex lenses may vary from 400 to 800 grams, sometimes as much as 1500 grams. Algorithmic solutions for the aberration problem were proposed (Powell, 1981; Farrar et al., 2000; Millan et al., 2006; Fang et al., 2006).

Chromatic aberrations in distorted images can be computationally corrected with two methods: with the blind or semi-blind deconvolution using PSF estimation, and with a contour analysis in different color channels (Chung et al., 2010). In (Kang, 2007), a combination of these two is used.

Aberration model in this case is derived as a generalization of an optical system defocus model. Well known Richardson and Lucy proposed an iteration deconvolution method for optical defocus compensation in astronomical observations. In recent years, a modified approach was used to correct chromatic aberration (Kang, 2007; Cho et al., 2010; Cho et al., 2012).

We use both correction methods to improve images obtained with Fresnel lenses. This type of lens (Soifer, 2012) can be defined as a stepped approximation of the Fresnel lens (Fig. 1), when a Fresnel lens is created by consecutive etching with different binary masks.

Fresnel lenses have advantages over refractive lenses in weight and linear size, especially pronounced for long focal lengths, where a single Fresnel lens can replace a complex set of refractive lenses. However, this comes at a cost: resulting images are blurred depending on the light wavelength and have multiple distortions such as moiré. As a result, Fresnel lenses are typically used as optical collimators or concentrators but not as imaging lens (Davis and Kuhnlenz, 2007).

Fresnel lenses have much stronger chromatic aberrations than simple refractive lenses do, which

Nikonorov A., Bibikov S., Petrov M., Yuzifovich Y. and Fursov V..
Computational Correction for Imaging through Single Fresnel Lenses.
DOI: 10.5220/0005543300680075
In *Proceedings of the 12th International Conference on Signal Processing and Multimedia Applications* (SIGMAP-2015), pages 68-75
ISBN: 978-989-758-118-2

need to be corrected in post-processing. One of the color channels (in this paper we use the green channel) has less blurring and can be used as a reference to correct the other two channels.

If color aberrations can be corrected, Fresnel lenses can be used as imaging lenses. In this paper we propose the model for correcting chromatic aberrations in the images obtained with Fresnel lenses, followed by the deconvolution, edge analysis and color correction. Finally, we present correction results for images captured using lens manufactured as a three-step approximation of Fresnel surface.

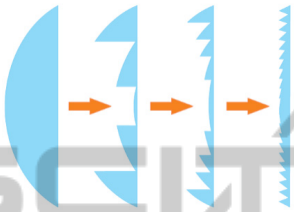

Figure 1: Conceptual illustration of collapsing aspheric refraction lens into Fresnel lens.

2 IMAGE CORRECTION FOR FRESNEL LENSES

A Fresnel lens typically adds a strong chromatic distortion in the non-monochromatic light. For any wavelength further away from the base wavelength λ_0, diffraction efficiency of the zero order decreases. The light focused in the zero order creates an additional chromatic highlight. This highlight becomes stronger as the wavelength deviates from λ_0. Diffraction efficiency of zero order can be expressed as:

$$\tau = \tau_0 \cos^2\left[(n-1)h\pi\lambda^{-1}\right], \quad (1)$$

where τ is transmittance coefficient in the zero order direction, τ_0 total lens transmittance coefficient, h - height of Fresnel lens microrelief, n – refraction index. We will call the color highlights caused by the energy focused in non-working diffraction orders as chromatic shift, in addition to the chromatic aberration. Chromatic aberration leads to color fringe along the edges and the color shift distorts colors of uniform colored areas of the image.

Chromatic aberration in refraction lenses is described by the general defocus model (Heide et al., 2013). In this model, the point spread function (PSF) is supposed to be linear, at least in the local spatial area, as shown in:

$$p^B_{RGB}(\mathbf{x}) = \mathbf{B} \otimes p^0_{RGB}(\mathbf{x}) + \mathrm{n}, \quad (2)$$

where $p^B_{RGB}(\mathbf{x})$ is the one of color channels of the blurred image, and $p^0_{RGB}(\mathbf{x})$ is the corresponding channel of the underlying sharp image, $\mathbf{B}$ is a blur kernel, or PSF, n is additive image noise, $\mathbf{x} \in Z^2_+$ is a point in image spatial domain.

Paper (Shih et al., 2012) shows that the lens PSF varies substantially being a function of the aperture, the focal length, the focusing distance, and the illuminant spectrum. So, a blur kernel $\mathbf{B}$ in (2) being a constant is not accurate enough, especially for Fresnel lenses with strong chromatic aberration.

For this strong aberration, a kernel $\mathbf{B}$ is space-varying. There are two distortion types in the image: a space-varying blur along the edges and a color shift in the regions with plain colors. Therefore, to handle these distortions, we use the following modification of (2):

$$p^{D,B}_{RGB}(\mathbf{x}) = \mathbf{B}_{RGB} \otimes p^D_{RGB}(\mathbf{x}) + \mathrm{n}, \quad (3)$$

$$p^D_{RGB}(\mathbf{x}) = D_{RGB}\left(p^0_{RGB}(\mathbf{x})\right). \quad (4)$$

Here $p^{D,B}_{RGB}(\mathbf{x})$ are color channels of the image captured with Fresnel lens; $D_{RGB}\left(p^0_{RGB}(\mathbf{x})\right)$ is a component characterizing the color shift, caused by the energy redistribution between diffraction orders. Blurring kernels $\mathbf{B}_{RGB}$ in (3) are different for different color channels; let us call these kernels the chromatic blur.

According to (3), the correction consists of two stages – removing the chromatic blur and the correction of the color shift. To correct chromatic blur we will use both deconvolution and sharpening. At first, we obtain a deblurred green channel, the sharpest one, by a deconvolution:

$$p^D_G(\mathbf{x}) = \mathbf{B}^{-1}_G \otimes \left(p^{D,B}_G(\mathbf{x})\right) \quad (5)$$

Here operation $\mathbf{B}^{-1}_G \otimes$ is a deconvolution for the chromatic deblurring, with an intermediate image $\mathbf{p}^D_G(\mathbf{x})$ as a result.

Then we apply sharpening to red and blue channels using the deblurred green channel as the guidance image:

$$p^D_{RB}(\mathbf{x}) = S\left(p^{D,B}_{RB}(\mathbf{x}), p^D_G(\mathbf{x})\right). \quad (6)$$

Finally, we apply color correction to the obtained image:

$$p_{RGB}(\mathbf{x}) = F\left(p^D_{RB}(\mathbf{x}), p^D_G(\mathbf{x})\right). \quad (7)$$

$F\left(p_{RB}^{D}(\mathbf{x}), p_{G}^{D}(\mathbf{x})\right)$ is a color correction transformation. Similar to sharpening, we use information available in the green channel to correct color shift in red and blue channels.

Combining the above steps, we propose the following technique based on model (3)-(4):

1) the chromatic deblurring (5) of the green channel based on the deconvolution, described in Section 3);

2) the chromatic sharpening (6) of the blue and red channels using the contours analysis (this approach is described in Section 4);

3) the color correction (7) to remove color shift, which is described in Section 5.

3 DECONVOLUTION BASED CHROMATIC DEBLURRING

To solve the image deconvolution problem (6), we base our optimization method on the optimal first-order primal-dual framework by Chambolle and Pock (Chambolle and Pock, 2011), whose original paper we recommend for an in-depth description. In this section, we present a short overview of this optimization.

Let X and Y be finite-dimensional real vector spaces for the primal and dual space, respectively. Consider the following operators and functions:

$\mathbf{K}: \mathrm{X} \to \mathrm{Y}$ is a linear operator from X to Y;

$\mathbf{G}: \mathrm{X} \to [0,+\infty)$ is a proper, convex, (l.s.c.) function;

$\mathbf{F}: \mathrm{Y} \to [0,+\infty)$ is a proper, convex, (l.s.c.) function, where l.s.c. stands for lower-semicontinuous.

The optimization framework considers general problems of the form

$$\hat{\mathbf{x}} = \arg\min_{\mathbf{x}} \mathbf{F}\left(\mathbf{K}(\mathbf{x})\right) + \mathbf{G}(\mathbf{x}) \tag{8}$$

To solve the problem in the form (8), the following algorithm is proposed in the paper (Chambolle and Pock, 2011).

Initialization step: choose - $\tau, \sigma \in R_{+}$, $\theta \in [0,1]$, $(\mathbf{x}_0, \mathbf{y}_0) \in \mathrm{X} \times \mathrm{Y}$ – some initial approximation, $\bar{\mathbf{x}}_0 = \mathbf{x}_0$.

Iteration step: $n \geq 0$, iteratively update $\mathbf{x}_n, \mathbf{y}_n, \bar{\mathbf{x}}_n$ as follows:

$$\mathbf{y}_{n+1} = prox_{\sigma F^*}\left(\mathbf{y}_n + \sigma \mathbf{K} \bar{\mathbf{x}}_n\right) \tag{9}$$

$$\mathbf{x}_{n+1} = prox_{\tau \mathbf{G}}\left(\mathbf{x}_n + \tau \mathbf{K}^* \mathbf{y}_{n+1}\right) \tag{10}$$

$$\bar{\mathbf{x}}_{n+1} = \mathbf{x}_{n+1} + \theta\left(\mathbf{x}_{n+1} - \mathbf{x}_n\right) \tag{11}$$

Following paper (Chung et al., 2010), a proximal operator with respect to **G** in (8), is:

$$\begin{aligned} prox_{\tau \mathbf{G}}(\hat{\mathbf{x}}) &= \left(\mathbf{E} + \tau \partial \mathbf{G}\right)^{-1}(\hat{\mathbf{x}}) = \\ &= \arg\min_{\mathbf{x}} \frac{1}{2\tau}\left\|\mathbf{x} - \hat{\mathbf{x}}\right\|_2^2 + \mathbf{G}(\mathbf{x}), \end{aligned} \tag{12}$$

where **E** is identity matrix. The proximal operator in (9) $prox_{\sigma F^*}$ is the same.

In order to apply the described algorithm to the deconvolution model, we follow (Chambolle, 2011):

$$\mathrm{F}(\nabla i) = \|\nabla i\|_1 \tag{13}$$

$$G(i) = \|\mathbf{B} \otimes i - j\|_2^2 \tag{14}$$

Using (13) and (14), it is possible to obtain the proximal operators for steps (9) and (10) of the algorithm. Further details are available in (Chambolle, 2011). The deconvolution algorithm based on the total variance can preserve sharp edges.

This deconvolution step is applied to the sharpest channel of the distorted image. The other two channels are restored using an edge processing procedure described in the next section.

4 COLOR CONTOURS PROCESSING

We propose a modification of the algorithm (Chung et al., 2010) to sharpen red and blue channels based on the deblurred green channel. This algorithm makes transition areas along the edges in red and blue channels look similar to transition areas in the green channel. An example of this area is shown in Fig. 2. For this algorithm to work properly, edges must be achromatic. While this is not always the case, we must rely on this assumption because we need to get strong chromatic blur removed in red and blue channels.

The original algorithm is based on the contour analysis. One of the color channels is used as a reference channel, a green channel in our case. Here we will consider one row of the image pixels with fixed x_2. Below in this section we will use one-dimensional indexing for clarity.

We will search for the edges in the green channel. Let x_c be the first detected transition point in the green channel, such as $\left|\nabla p_G(x_c)\right| \geq T$, where T – a threshold value. Let us consider a neighborhood of $x_c - N$:

$$B(x) = \max_{x \in N} sign\left(\nabla p_G(x_c)\right) \nabla p_{RGB}(x). \quad (15)$$

The required transition zone $N_C(x_c)$ is defined as follows:

$$N_C(x_c) = \{x : B(x) \geq \mathrm{T}, x \neq x_c\}. \quad (16)$$

Let l_C be the left border, and r_C be the right border of this area.

In the transition area, an abrupt change of values in red or blue or both color channels occurs. The algorithm transforms signals in red and blue channels to match the signal in the green channel in the transition area $N_C(x_c)$ as closely as possible.

To do this, we define differences between signals:

$$d_{RB}(x) = p_{RB}(x) - p_G(x). \quad (17)$$

For each pixel $x \in N_C$, these differences must be smaller than the differences on the border of the transition area. If this is not the case, red and blue components of these pixels need to be corrected in one of the following ways.

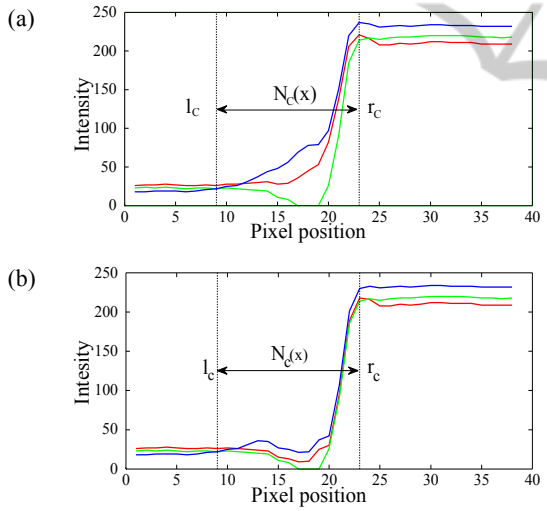

Figure 2: Algorithm output results: (a) an original image (b) an image after color contour processing.

The signal $S_{RB}(x)$ depends on the color difference between channels (17) at a pixel $x \in N_C$:

$$\begin{cases} \max\left(d_{RB}(l_C), d_{RB}(r_C)\right) + p_G(x), \\ \text{if } d_{RB}(x) \geq \max\left(d_{RB}(l_C), d_{RB}(r_C)\right); \\ \min\left(d_{RB}(l_C), d_{RB}(r_C)\right) + p_G(x), \\ \text{if } d_{RB}(x) \leq \min\left(d_{RB}(l_C), d_{RB}(r_C)\right); \\ 0, \quad \text{else}. \end{cases} \quad (18)$$

Therefore, color differences d_{RB} decrease, and the red and blue signals in the transition area look more similar to the green signal. An example of the algorithm output is shown in Fig. 2(b).

The energy of the red and blue channels can be low or high compared to the green channel. We can define normalization constants c_{RB} to reduce this imbalance. c_{RB} are defined as a ratio of per pixel energy in the red and blue channels to the energy in the green channel. So, (17) takes the following form:

$$d^n_{RB}(x) = (p_{RB}(x) - p_G(x)) c_{RB}. \quad (19)$$

After replacing d_{RB} with d^n_{RB} $S_{RB}(x)$ takes the following form:

$$\begin{cases} \min\left(d^n_{RB}(l_C), d^n_{RB}(r_C)\right) + p_G(x), \\ \text{if } d^n_{RB}(x) \leq \min\left(d^n_{RB}(l_C), d^n_{RB}(r_C)\right); \\ \max\left(d^n_{RB}(l_C), d^n_{RB}(r_C)\right) + p_G(x), \\ \text{if } d^n_{RB}(x) > \max\left(d^n_{RB}(l_C), d^n_{RB}(r_C)\right). \end{cases} \quad (20)$$

If pixel luminosity in the red and blue channels in transition regions is close to zero, we replace it with the middle value in a neighboring window.

There are several pixels with close to zero values in the green channel, pixels #16-19 in Fig. 2(a). This means that there is no significant information in the green channel for pixel correction in the red and blue channels in this part of the transition area. We propose the following algorithm to solve this problem:

1) We use a median filter to preprocess the green channel in order to handle close to zero values. We replace a pixel with a close to zero value to the middle value in a neighboring window. If the new value is also close to zero, the window size of the median filter increases.

2) We compute the matrix of the correction coefficients $R_{RB}(\mathbf{x})$ for the whole image. Then we apply the post processing steps 3) and 4) to the $R_{RB}(\mathbf{x})$ values.

3) We apply grayscale dilation (Gonzalez and Woods, 2001) to matrices of sharpening values $S_{RB}(\mathbf{x})$.

4) We limit excessively bright pixels to values allowed inside the transition area.

Finally we sharpen red and green channels using the following rule:

$$p^D_{RB}(\mathbf{x}) = \begin{cases} S_{RB}(\mathbf{x}), & S_{RB}(\mathbf{x}) \neq 0; \\ p^{D,B}_{RB}(\mathbf{x}), & S_{RB}(\mathbf{x}) = 0. \end{cases} \quad (21)$$

After deblurring of the green channel and sharpening of the red and blue channels, we use color correction, described in the following section, to remove the strong color shift caused by the energy redistribution between diffraction orders.

5 COLOR SHIFT CORRECTION

The proposed chromatic aberration correction includes color correction in its final stage. A detailed description of the color correction approach is provided in (Nikonorov et al., 2014). This correction problem consists of correcting non-isoplanatic deviation in illumination $I(\lambda,\mathbf{x})$ and restoring an image with the given illumination $I_0(\lambda)$:

$$\begin{aligned}&\mathbf{p}(\mathbf{x})=\int R(\lambda,\mathbf{x})I(\lambda,\mathbf{x})\mathbf{T}(\lambda,\mathbf{x})d\lambda\rightarrow\\&\rightarrow\mathbf{p}_0(\mathbf{x})=\int R(\lambda,\mathbf{x})I_0(\lambda)\mathbf{T}(\lambda)d\lambda,\end{aligned}\tag{22}$$

where R and I are $R\times Z_2\rightarrow[0,1]$ functions of the wavelength λ. R is the spectral reflectance of the scene surfaces. I is the spectral irradiance that is incident at each scene point. $\mathbf{T}(\lambda)=\left[T^{\{1\}}(\lambda),...,T^{\{K\}}(\lambda)\right]^T$ is the spectral transmittance distribution of color sensors. In (Nikonorov et al., 2014) it was shown that the task (22) could be solved by finding the correction function.

We propose using prior knowledge of the colors of small isolated patches in the image in the same way as any color correction specialist would do. These small neighborhoods, limited in color and space, are defined in (Nikonorov et al., 2014) as *color shape elements*, CSE. This model was useful for both, color correction and artefact removing problems (Nikonorov et al., 2010).

Using CSE, the task of the correction function identification takes the following form:

$$\mathbf{a}^*=\arg\min_{\mathbf{a}}\left\|F(\mathbf{u}_i,\mathbf{a}),\mathbf{u}_i^0\right\|\tag{23}$$

where $\{\mathbf{u}_i\}$ is a set of distorted CSE, and $\{\mathbf{u}_i^0\}$ is a set of distortion-free CSE. Hausdorff-like measure between CSEs in three dimensional color space is used as a metric $\|\ ,\ \|$ in (23). A general form for this metric is:

$$\left\|\mathbf{u}_i,\mathbf{u}_j\right\|=\max\begin{pmatrix}\max\limits_{\mathbf{x}\in\mathbf{u}_i}\min\limits_{\mathbf{y}\in\mathbf{u}_j}\left|\mathbf{p}(\mathrm{x}),\mathbf{p}(\mathrm{y})\right|,\\\max\limits_{\mathbf{y}\in\mathbf{u}_j}\min\limits_{\mathbf{x}\in\mathbf{u}_i}\left|\mathbf{p}(\mathrm{x}),\mathbf{p}(\mathrm{y})\right|\end{pmatrix},\tag{24}$$

where $|\ ,\ |$ is a distance in color space. We use a separate parameter estimation (23) for each color channel.

Since we use a channel-wise correction procedure, the metric (19) can be calculated using only two values for each color channel independently, and (18) takes the following form for each color channel p:

$$\begin{cases}\mathbf{a}^*=\arg\min_{\mathbf{a}}\left\|F(p_k,\mathbf{a}),p_k^0\right\|,\\\mathrm{p}_k=\min p(\mathbf{u}_i),\ \mathrm{p}_{k+1}=\max p(\mathbf{u}_i),\\\mathrm{p}_k^0=\min p(\mathbf{u}_i^0),\ \mathrm{p}_{k+1}^0=\max p(\mathbf{u}_i^0).\end{cases}\tag{25}$$

Here we assume that the distortions are described by a modified dichromatic model (Maxwell et al., 2008) of the following form:

$$\begin{aligned}p_{RGB}(\mathbf{x})=\int\big[&H(\mathbf{x})I(\lambda)R_B(\lambda,\mathbf{x})+\\&+I_A(\lambda)R_B(\lambda,\mathbf{x})+D_{RGB}(\lambda)\big]\mathbf{T}(\lambda)d\lambda,\end{aligned}\tag{26}$$

where $I(\lambda)R(\lambda,\mathbf{x})$ is the diffuse reflection, $I(\lambda,\mathbf{x})R_S(\lambda,\mathbf{x})$ is the specular reflection, and the ambient light is $I_A(\lambda)$, $H(\mathbf{x})$ is the attenuation factor, and $D_{RGB}(\lambda)$ is added to describe the color shift caused by energy redistribution between diffraction orders. We use this model for correction identification using calibration tables so specular reflection is ignored in our case.

For the distortions described by this model, the CSE matching condition theorem from (Nikonorov et al., 2014) could be proven with constraints on the ambient light. Using necessary condition from this theorem, the identification problem of the correction function takes the following form:

$$\begin{cases}\mathbf{a}^*=\arg\min_{\mathbf{a}}\left(\left(F(p_k,\mathbf{a})-p_k^0\right)^2\right),\\F'(p_k,\mathbf{a})\geq 0.\end{cases}\tag{27}$$

In the problem of color correction for Fresnel lenses, we use a color checker scale, shown in Fig. 4(c, f), for correction identification of each color channel. The original colors of the scale are used as distortion-free CSE, $\mathbf{u}_i^0$. The same scale captured using a Fresnel lens is used for getting distorted CSEs, $\mathbf{u}_i$.

As shown in (Nikonorov et al., 2014), the problem (27) could be solved for polynomial representation of $F(\ )$. However, the distortions caused by the aberrations in the simple Fresnel lens are too strong. To improve color correction quality, we apply additional conditions.

First, we add two boundary conditions for $F(\ )$: setting it to zero at the starting point, while setting it to one at the end:

$$F(0,\mathbf{a})=0, \quad F(1,\mathbf{a})=1. \tag{28}$$

Because these conditions cannot be applied to a polynomial representation of $F(\ )$, we use cubic smoothed splines with boundary conditions (28).

Second, as shown in Fig. 3, an initial SSEs set is too noisy, and some data points must be dropped. A classic algorithm for noisy data selection with dropping outliers is RANSAC algorithm. We use a slightly modified RANSAC-based scheme:

1) Select a subset of the initial set.

2) Using this subset, estimate cubic smoothing spline parameters for $F(\ )$ according to (26)-(27).

3) For each pair of SSEs, the following inequality can be computed:

$$\left\| F(\mathbf{u}_i,\mathbf{a}),\mathbf{u}_i^0 \right\| \le t, \tag{29}$$

where t is a threshold. Inequality (29) is true for inlayer CSEs pairs and false for outliers.

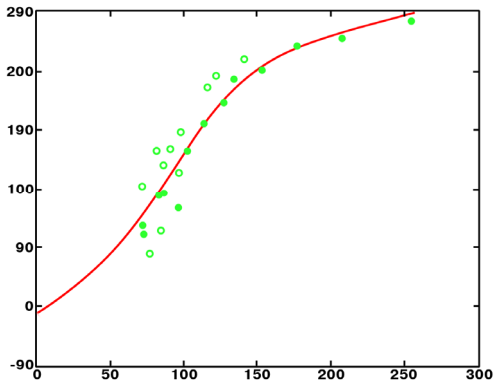

Figure 3: Chromatic shift correction curve for the green channel, solid points for inlayers CSEs, pitted – for outliers.

After identifying color correction transform parameters we apply this transform to the image as the final step of the technique based on model (3)-(4).

To check correction quality we use the following measure:

$$q=\max_i \max_{\mathbf{x}_j\in\mathbf{u}_i} \left\| \mathbf{p}_0(\mathbf{x}_j),\mathbf{p}(\mathbf{x}_j) \right\|_2, \tag{30}$$

where $\|\ ,\ \|_2$ is Euclidian distance between colors of corresponding points of two CSEs – source $\mathbf{p}_0(\mathbf{x}_j)$ and corrected $\mathbf{p}(\mathbf{x}_j)$. We know the matching between the source and the corrected point for color checker tables. This usually unavailable knowledge allows us to estimate the value of quality measure (30), and we will use this measure to evaluate correction quality.

6 RESULTS

The results of the correction are shown in Fig. 4. The original picture was captured using a simple, wich was made as three-step approximation of the Fresnel lens. First we removed the blur from the green channel using deconvolution, and then we used edge analysis for the red and blue channels. Color correction transform was identified using color checker table (Fig. 4(c, f)), and finally color correction was applied to the image.

As shown in Fig. 4, the proposed correction technique restores both colors and edge information from distorted images, captured by a simple Fresnel lens. We compared our color correction technique with an implementation of Retinex approach from (Limare et al., 2011). Results for Retinex-based correction are shown in Fig. 4(e). Visual quality of color correction exceeds the quality of the Retinex-based correction. The value of the quality measure (30) for Retinex is 113 versus 14 for our method.

7 CONCLUSIONS

We show that a simple Fresnel lens can be used for imaging. Strong aberrations inherent in this optical system can be restored by digital image processing. Images captured with a simple Fresnel lens are corrected with deconvolution and contour analysis with good results. After we applied deconvolution for deblurring of the typically less blurred green channel, we then sharpened the image for other color channels taking green channel as the guidance image.

After deblurring and sharpening we applied color correction to remove strong chromatic shift. Correction transformation was identified using color checker tables. These tables help to quantify correction quality, and the proposed correction technique shows a better quality than the well-known Retinex method of color correction.

For further research, we see two main directions

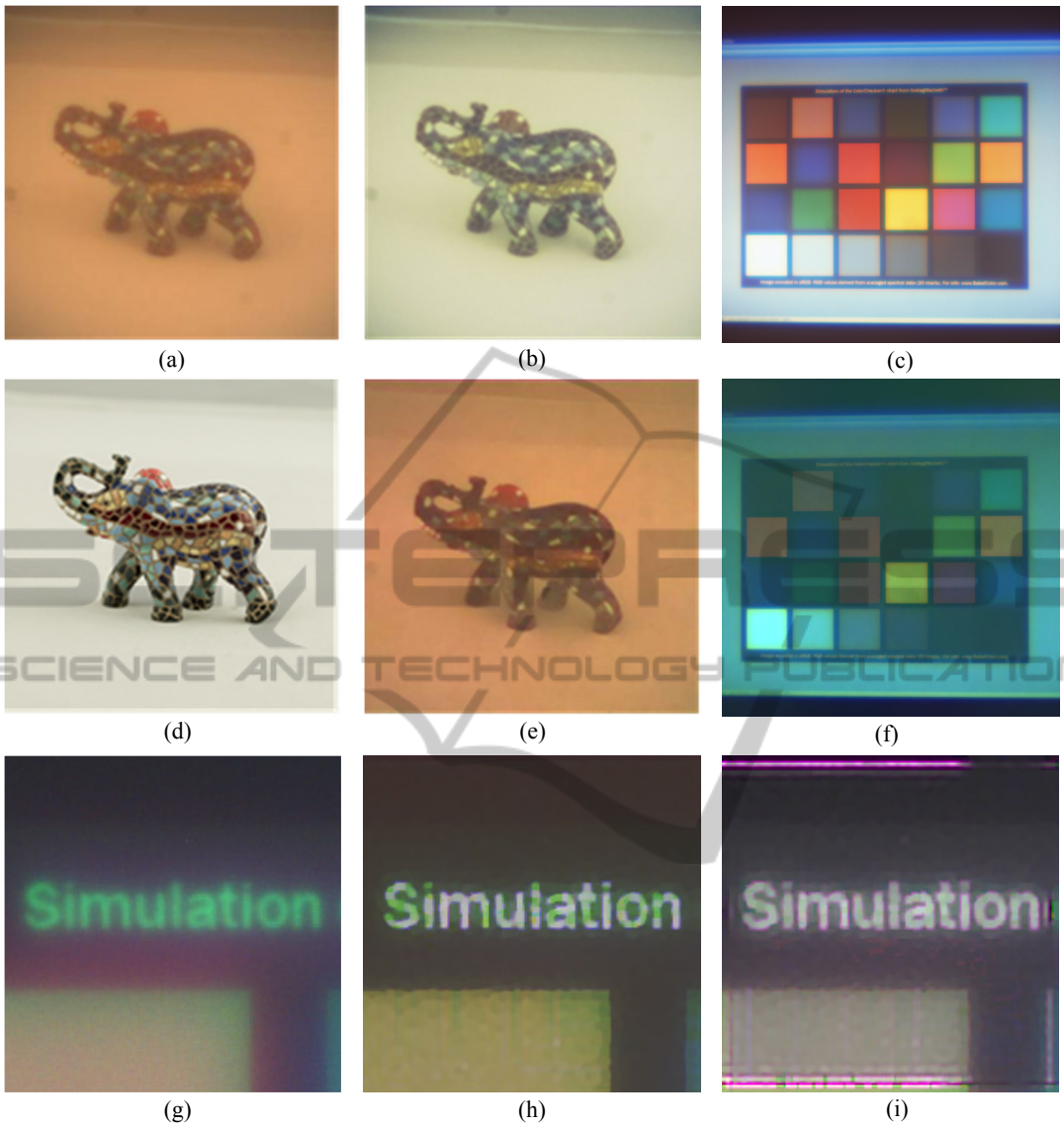

Figure 4: Example of chromatic aberration correction: (a) - image captured by four-step Fresnel lens, (b) - image after color correction, (d) - image captured by refraction lens, (e) - image after Retinex-based color correction; (c) - color checker image for correction identification, and (f) - color checker image after correction; (g) - part of color chart, captured by four-step Fresnel lens, (h) - same part after computational correction, (i) – after final color sharpening.

that may yield additional quality improvements: 1) increasing the quality of deconvolution, taking into account the estimation of space-varying PSF and 2) combining edge analysis and color correction to a single filter.

ACKNOWLEDGEMENTS

This work was partially supported by project #RFMEFI57514X0083 by the Ministry of Education and Science of the Russian Federation.

REFERENCES

Chambolle, A., & Pock, T., 2011. A first-order primal-dual algorithm for convex problems with applications to imaging. *Journal of Mathematical Imaging and Vision*, vol. 40, no. 1, pp. 120–145.

Cho, T. S., Joshi, N., Zitnick, C. L., Sing Bing Kang, Szeliski, R., & Freeman, W.T., 2010. A content-aware image prior *IEEE Conference on Computer Vision and Pattern Recognition*, pp. 169-176.

Cho, T. S., Zitnick, C. L., Joshi, N., Sing Bing Kang, Szeliski, R., & Freeman, W.T., 2012. Image restoration by matching gradient distributions. *IEEE Transactions on Pattern Analysis and Machine Intelligence*, vol. 34, no. 4, pp. 683-694.

Chung, S.-W., Kim, B.-K., & Song, W.-J., 2010. Removing chromatic aberration by digital image processing. *Optical Engineering*, vol. 49, no. 6, 067002.

Davis, A., & Kuhnlenz, F., 2007. Optical design using Fresnel lenses - basic principles and some practical examples. *Optik & Photonik*, vol. 2, no. 4, pp. 52–55.

Fang, Y. C., Liu, T. K., MacDonald, J., Chou, J. H., Wu, B. W., Tsai, H. L., & Chang, E. H., 2006. Optimizing chromatic aberration calibration using a novel genetic algorithm. *Modern Optics*, v. 53, no. 10, pp. 1411-1427.

Farrar, N. R., Smith, A. H., Busath, D. R., & Taitano, D., 2000. In situ measurement of lens aberration. *Proc. SPIE*, vol. 4000, March, pp. 18-29.

Gonzalez, R. C., & Woods, R. E., 2001. *Digital Image Processing*, Second Edition, Prentice Hall, 2001.

Heide, F., Rouf, M., Hullin, M. B., Labitzke, B., Heidrich, W., & Kolb, A., 2013. High-quality computational Imaging Through Simple Lenses. *ACM Transactions on Graphics,* vol. 32, no. 5, article No. 149.

Kang, S. B., 2007. Automatic removal of chromatic aberration from a single image. *Computer Vision and Pattern Recognition, 2007*, pp. 1-8.

Limare, N., Petro, A. B., Sbert, C., & Morel, J. M., 2011. Retinex Poisson equation: a model for color perception. *Image Processing On Line*.

Maxwell, B. A., Friedhoff, R. M., & Smith, C. A., 2008. A bi-illuminant dichromatic reflection model for understanding images. *Computer Vision and Pattern Recognition, IEEE Conference on*, pp. 1–8.

Meyer-Arendt, J. R., 1995. *Introduction to Classical and Modern Optics*. Prentice Hall.

Millan, M. S., Oton, J., & Perez-Cabre, E., 2006. Chromatic compensation of programmable Fresnel lenses. *Opics Express*, vol. 14, no. 13, pp. 6226-6242.

Nikonorov, A., Bibikov, S., & Fursov V., 2010. Desktop supercomputing technology for shadow correction of color images. *Proceedings of the 2010 International Conference on Signal Processing and Multimedia Applications (SIGMAP)*, pp. 124-140.

Nikonorov, A., Bibikov, S., Yakimov, P., & Fursov, V., 2014. Spectrum shape elements model to correct color and hyperspectral images. *8th IEEE IAPR Workshop on Pattern Recognition in Remote Sensing*, *2014*, pp. 1-4.

Powell, I., 1981. Lenses for correcting chromatic aberration of the eye. *Applied Optics*, v. 20, no. 24, pp. 4152–4155.

Shih, Y., Guenter, B., & Joshi N., 2012. Image enhancement using calibrated lens simulations. *Computer Vision – ECCV 2012*, pp. 42-56.

Soifer, V. A. (ed.), 2012. *Computer Design of Diffractive Optics*. Woodhead Publishing.